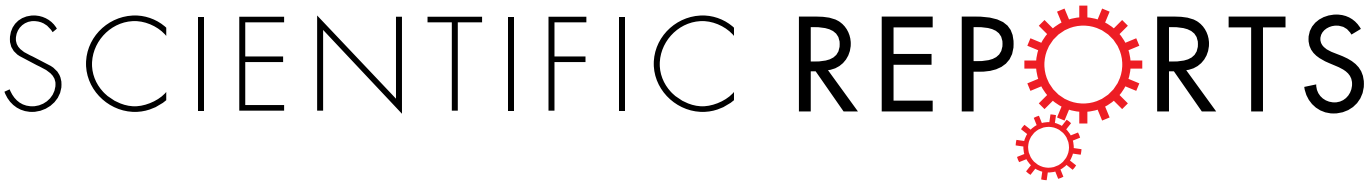

OPEN

hiPSC-derived cardiomyocytes from Brugada Syndrome patients without identified mutations do not exhibit clear cellular electrophysiological abnormalities

Received: 08 January 2016
Accepted: 11 July 2016
Published: 03 August 2016

Christiaan C. Veerman[1,*], Isabella Mengarelli[1,*], Kaomei Guan[2], Michael Stauske[2], Julien Barc[1,3], Hanno L. Tan[1], Arthur A. M. Wilde[1], Arie O. Verkerk[4,*] & Connie R. Bezzina[1,*]

Brugada syndrome (BrS) is a rare cardiac rhythm disorder associated with sudden cardiac death. Mutations in the sodium channel gene *SCN5A* are found in ~20% of cases while mutations in other genes collectively account for <5%. In the remaining patients the genetic defect and the underlying pathogenic mechanism remain obscure. To provide insight into the mechanism of BrS in individuals without identified mutations, we here studied electrophysiological properties of cardiomyocytes (CMs) generated from human induced pluripotent stem cells (hiPSCs) from 3 BrS patients who tested negative for mutations in the known BrS-associated genes. Patch clamp studies revealed no differences in sodium current (I_{Na}) in hiPSC-CMs from the 3 BrS patients compared to 2 unrelated controls. Moreover, action potential upstroke velocity (V_{max}), reflecting I_{Na}, was not different between hiPSC-CMs from the BrS patients and the controls. hiPSC-CMs harboring the BrS-associated *SCN5A*-1795insD mutation exhibited a reduction in both I_{Na} and V_{max}, demonstrating our ability to detect reduced sodium channel function. hiPSC-CMs from one of the BrS lines demonstrated a mildly reduced action potential duration, however, the transient outward potassium current (I_{to}) and the L-type calcium current ($I_{Ca,L}$), both implicated in BrS, were not different compared to the controls. Our findings indicate that ion channel dysfunction, in particular in the cardiac sodium channel, may not be a prerequisite for BrS.

Brugada syndrome (BrS) is a rare inheritable cardiac disorder characterized by ST-segment elevation and a negative T-wave in leads V1–V3 of the ECG and an increased risk of sudden cardiac death from ventricular fibrillation (VF)[1,2]. In spite of intense research by means of clinical, experimental and genetic studies, the basis for these ECG abnormalities and the mechanism underlying VF in this disorder are incompletely understood.

The *SCN5A* gene, mutated in ~20% of BrS probands[3], is thus far the only gene that has unequivocally been associated with the disorder[4]. *SCN5A* encodes the major sodium channel isoform in heart (Na_v 1.5), which underlies the cardiac Na^+ -current (I_{Na}) responsible for rapid cardiomyocyte depolarization and as such is a key player in cardiac conduction[5]. BrS causing mutations in *SCN5A* result in loss of I_{Na} and are thought to contribute to the disorder through the slowing of conduction, a mechanism that is believed to be central in the pathogenesis of the disorder[6]. Mutations in other genes have been found in a small percentage of BrS patients; these encode proteins that modulate I_{Na} (interacting proteins or beta-subunits) or lead to the loss- or gain-of-function of the L-type Ca^{2+} -current ($I_{Ca,L}$) or the outward K^+ -currents (I_{KATP} and I_{to}), respectively[2]. In the vast majority of BrS patients, however, no causal mutation is identified and studies investigating comprehensive lists of genes encoding candidate ion channel genes and their modulatory subunits have not uncovered strong associations with the disorder[7].

[1]Heart Centre, Department of Experimental and Clinical Cardiology, Academic Medical Center, University of Amsterdam, Amsterdam, The Netherlands. [2]Department of Cardiology and Pneumonology, Georg-August-University Göttingen, Göttingen, Germany. [3]l'institut du thorax, INSERM, CNRS, Université de Nantes, Nantes, France. [4]Department of Anatomy, Embryology and Physiology, Academic Medical Center, University of Amsterdam, Amsterdam, The Netherlands. *These authors contributed equally to this work. Correspondence and requests for materials should be addressed to C.R.B. (email: C.R.Bezzina@amc.uva.nl)

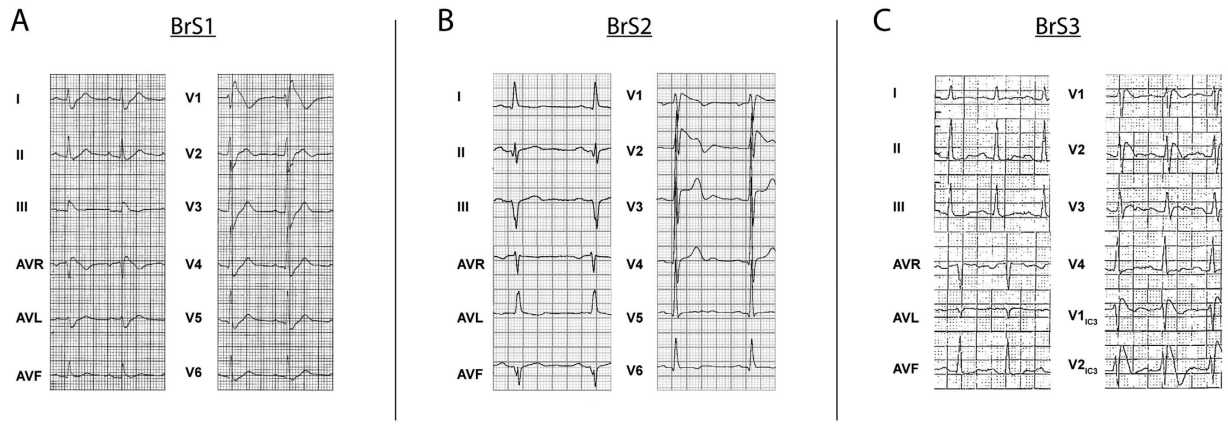

Figure 1. Electrocardiogram (25 mm/s, 10 mm/mv) of BrS1 (**A**), BrS2 (**B**) and BrS3 (**C**). Type 1 BrS signs are visible in leads V1–V2 (**A,B**) or $V1_{IC3}$–$V2_{IC3}$ (**C**) (leads positioned the 3rd intercostal space cranial from V1 and V2).

In these patients it remains unclear whether the disorder is caused, at least in part, by an ion channel defect or whether the disorder is caused to a large part by other factors. Such other factors may be extrinsic to the cardiomyocyte, such as the deposition of fibrosis, or may involve defects of cardiomyocyte electrical coupling through gap junctions, the relevance of which is increasingly recognized[8–10].

The possibility to generate cardiomyocytes (CMs) from human induced pluripotent stem cells (hiPSCs, hiPSC-CMs) from patient material provides the opportunity to study the electrophysiological characteristics of patient-specific cardiomyocytes, with the possibility of gleaning insights into disease mechanisms[11]. In this study we generated hiPSC-CMs from three unrelated BrS patients that were negative for coding region mutations in BrS-associated genes and compared their electrophysiological properties to hiPSC-CMs from two unrelated control individuals. We demonstrate that hiPSC-CMs from the three BrS patients do not exhibit Na^+ channel dysfunction and that action potential (AP) characteristics do not point towards a clear cellular electrophysiological defect. hiPSC-CMs from one of the BrS lines demonstrated a mild reduction in AP duration, however, neither I_{to} nor $I_{Ca,L}$ differed significantly from hiPSC-CMs from the two controls. This supports the hypothesis that ion channel dysfunction, in particular in the cardiac sodium channel, may not be a prerequisite for BrS.

Results

Patient characteristics. BrS was diagnosed following the 2005 consensus diagnostic criteria[12]. The 1st patient we included in this study (BrS1) was a 42-year-old male who presented at night with an out-of-hospital cardiac arrest based on VF. His medical history included unexplained syncope 2 years earlier, but was otherwise unremarkable. He took no medications and there was no obvious cause for VF. He had a type 1 BrS ECG (>2 mm coved-type ST-elevation and a negative T-wave) in lead V1 (Fig. 1A). QRS-duration was increased (120 ms) while the PR- and QTc-intervals were within the normal range. QTc intervals were determined in lead II from three consecutive complexes and corrected for heart rate according to Bazzett's formula[13]. Magnetic resonance imaging showed no structural abnormalities and coronary angiography demonstrated no coronary artery disease. His first- and second-degree relatives did not show baseline ECG abnormalities, however provocation with ajmaline evoked a type 1 BrS ECG in 3 out of 6 individuals tested. No history of sudden cardiac death was present in the patient's family.

The 2nd patient (BrS2) was a 67-year-old male with a history of syncope who presented with a type 1 BrS ECG during a hospital admission for an inferior myocardial infarction (Fig. 1B). His ECG showed a prolonged PR-interval (230 ms) with a normal QRS-duration and QTc-interval. Moreover, the patient had episodes of paroxysmal atrial fibrillation. During electrophysiological investigation ventricular arrhythmia could be evoked, after which an ICD was implanted. Apart from the proband, no relatives were identified with a type 1 BrS ECG at baseline, while flecainide provocation tests in 15 first- and second-degree relatives revealed 6 individuals fulfilling the ECG criteria of BrS. In the patient's family, sudden cardiac death was reported in several members.

The 3rd patient (BrS3) was a 24-year-old female who presented at the outpatient clinic because of episodes of syncope. She had a type 1 BrS ECG seen in ECG leads placed over the 3rd intercostal space cranially from V1 and V2 (Fig. 1C). Additional electrophysiological investigation revealed inducible non-sustained ventricular tachycardias in the right-ventricular outflow tract, after which an ICD was placed. Conduction parameters revealed PQ-interval prolongation (220 ms), with a normal QRS-duration and QTc interval. Screening of family members by ajmaline provocation revealed 5 individuals fulfilling the BrS ECG diagnostic criteria among 12 individuals tested in whom no ECG abnormalities were identified at baseline. No history of sudden cardiac death was reported in the family of the patient.

Genetic screening of the coding region of *SCN5A* did not uncover any novel or rare variants (MAF <1%) in the three patients. Moreover, BrS1 and BrS2 were negative for such variants in all other BrS-associated genes. BrS3 carried a rare variant in the *CACNA1C* gene (present in 5 of 120140 alleles in the ExAC database). However, this variant, which is present at position −7 of intron 19 (numbering according to Ensembl transcript ENST00000399634), does not appear to entail a nucleotide change that negatively affects splicing (pyrimidine to

pyrimidine change in the polypyrimidine tract), and analysis of the wild-type and variant sequence surrounding the 3′ splice site of intron 19 using three different splice site prediction programs[14–16] did not uncover any splicing motif alteration. This led us to conclude that this variant has probably no impact on splicing.

Generation of hiPSCs and hiPSC-CMs. Dermal fibroblasts from the three patients were reprogrammed into hiPSCs through lentiviral transduction of the transcription factors *OCT4*, *KLF4*, *SOX2*, *c-MYC*; the three lines thus generated are hereafter annotated as iBrs1-3 for patients BrS1, BrS2 and BrS3 respectively. The hiPSC lines showed alkaline phosphatase activity and stained positive for the pluripotency markers OCT4, SOX2, LIN28, SSEA-4 and Tra-1-60. (Supplementary Fig. 1A–C). Moreover, spontaneous differentiation resulted in the formation of cell types from the three germ layers, ectoderm, mesoderm and endoderm, as evidenced by immunostaining for the proteins β-III-Tubulin, α-SMA and AFP, respectively (Supplementary Fig. 2). The karyotypes of iBrs1-3 were normal (Supplementary Fig. 3). Differentiation of hiPSCs into CMs was confirmed by positive immunostainings of the cardiac markers NKX2.5 and cTNT (Supplementary Fig. 4)

Electrophysiological characteristics of hiPSC-CMs from Brugada Syndrome patients. Patch-clamp electrophysiological studies were conducted in hiPSC-CMs generated from the three BrS patients (iBrS1, iBrS2 and iBrS3) and in hiPSC-CMs from the two controls (iCtrl1 and iCtrl2). In addition, hiPSC-CMs derived from a patient with the 1795insD mutation in *SCN5A* (iSCN5A)[17] served as a positive control to demonstrate our ability to detect reduced I_{Na} function, and its consequences on the AP, in our experimental system.

Figure 2A shows representative traces of I_{Na} from all groups. Average peak I_{Na} of iBrS1, iBrS2 and iBrS3 hiPSC-CMs did not differ significantly from the two controls (Fig. 2B,C). In contrast, iSCN5A displayed a marked reduction in I_{Na} density ($p < 0.01$ versus iCtrl1 and iCtrl2; Fig. 2B,C). Voltage dependence of I_{Na} activation did not differ significantly between the groups (Fig. 2D and Table 1). Voltage dependence of inactivation of iBrS1, iBrS2 and iSCN5A did not differ significantly from iCtrl2, while iBrS3 displayed similar values as iCtrl1 (Fig. 2E and Table 1). The voltage dependence of inactivation of iCtrl1 and iCtrl2 differed significantly between each other, with iCtrl1 displaying a slight positive shift in $V_{1/2}$ of inactivation ($p < 0.05$; (Fig. 2E and Table 1). The time constants of current inactivation, determined at a test potential of −30 mV, were not different in iBrS1, iBrS2 and iBrS3 compared with the two controls. hiPSC-CMs from iSCN5A showed slower time dependence of current inactivation, in accordance with an increased late I_{Na} induced by the 1795insD mutation (Table 1) ($p < 0.01$).

Next, we measured APs in single hiPSC-CMs. As explained in detail in the Methods section this was done after *in silico* addition of I_{K1} (see Supplementary Fig. 5 for an example of computed I_{K1}). Fig. 3A shows typical APs stimulated at 1 Hz. Maximal AP upstroke velocity (V_{max}), reflecting I_{Na} function[18], was not significantly different between iCtrl1, iCtrl2, iBrS1, iBrS2 and iBrS3 (Fig. 3B). In contrast, iSCN5A demonstrated markedly reduced V_{max} ($p < 0.05$ versus iCtrl1 and iCtrl2), consistent with the reduced I_{Na} density (Fig. 2B). Maximal diastolic potential (MDP), AP plateau amplitude ($APA_{plateau}$) and action potential duration (APD) at 20, 50 and 80% of repolarization (APD_{20}, APD_{50} and APD_{80}, respectively) were not statistically significantly different between the various BrS groups and the controls, with exception of iBrS2, which displayed shorter APD compared to one of the two controls (iCtrl2, $p < 0.05$) (Fig. 3C). In addition, iSCN5A exhibited a marked increase in APD, AP maximal amplitude (APA_{max}) and $APA_{plateau}$, in line with an increased late I_{Na} that is induced by the mutation, as demonstrated previously[17]. Of note, all AP parameters in iCtrl1 and iCtrl2 were not different between each other ($p > 0.05$ for all parameters). No additional differences in V_{max}, APD and $APA_{plateau}$ were uncovered upon stimulation at frequencies of 0.5–3 Hz (Fig. 3E and Supplementary Fig. 6).

Given the shorter APD that was found in iBrS2 hiPSC-CMs, $I_{Ca,L}$ and I_{to} were measured in hiPSC-CMs from this cell line and compared with hiPSC-CMs from the two controls. Both these currents are implicated in BrS and could underlie the observed differences in APD. Fig. 4A shows typical traces of $I_{Ca,L}$ measured at a test potential of 0 mV. $I_{Ca,L}$ density was not affected in iBrS2 as compared to the two controls iCtrl1 and iCtrl2 (Fig. 4B). Also, voltage dependence of activation was not different between all groups, while iCtrl1 demonstrated a negative shift of 4 mV in voltage dependence of inactivation as compared to iCtrl2 ($p < 0.05$). Time constants of current inactivation, measured at a potential of 0 mV, were not statistically different between all groups (τ_{fast}: 4.0 ± 0.2, 3.7 ± 0.2 and 3.6 ± 0.3 ms in iCtrl1, iCtrl2 and iBrS2, respectively; τ_{slow} 18.2 ± 0.8, 21.5 ± 1.3 and 21.5 ± 1.4 in iCtrl1, iCtrl2 and iBrS2, respectively).

Figure 5A shows typical traces of I_{to} elicited at +40 mV. I_{to} was present in all cells measured and neither I_{to} densities (Fig. 5B) nor the voltage dependence of I_{to} (in)activation (Fig. 5C) were different between all groups. Moreover, there were no statistically significant differences in time constant of inactivation, as determined with a mono-exponential fit at a test potential of +40 mV. (τ: 28.1 ± 4.6, 26.0 ± 5.0 and 27.1 ± 3.3 ms in iCtrl1, iCtrl2 and iBrS2, respectively).

Discussion

In this study we used hiPSC technology to generate cardiomyocytes from three patients with BrS that did not carry coding region mutations in the known BrS-associated genes. By comparing their electrophysiological properties to those of cardiomyocytes derived from two control individuals as well as an individual carrying the established mutation *SCN5A*-1795insD as positive control, we aimed to glean insight into the underlying mechanism of BrS.

Although the evidence supporting causality varies across genes, at least 20 different genes have so far been implicated in BrS[2,3]. They all encode ion channel subunits or proteins that putatively modulate ion channel function. In accordance, functional studies on mutations within these genes have consistently invoked abnormal ion channel function as a contributory mechanism, namely through a reduction in I_{Na} or $I_{Ca\text{-}L}$, or through an increase in I_{to} and I_{KATP}. As such, these observations point to a cellular electrophysiological defect in at least a subset of BrS patients. Around 80% of patients however do not carry coding region mutations in these genes[3]. In these patients,

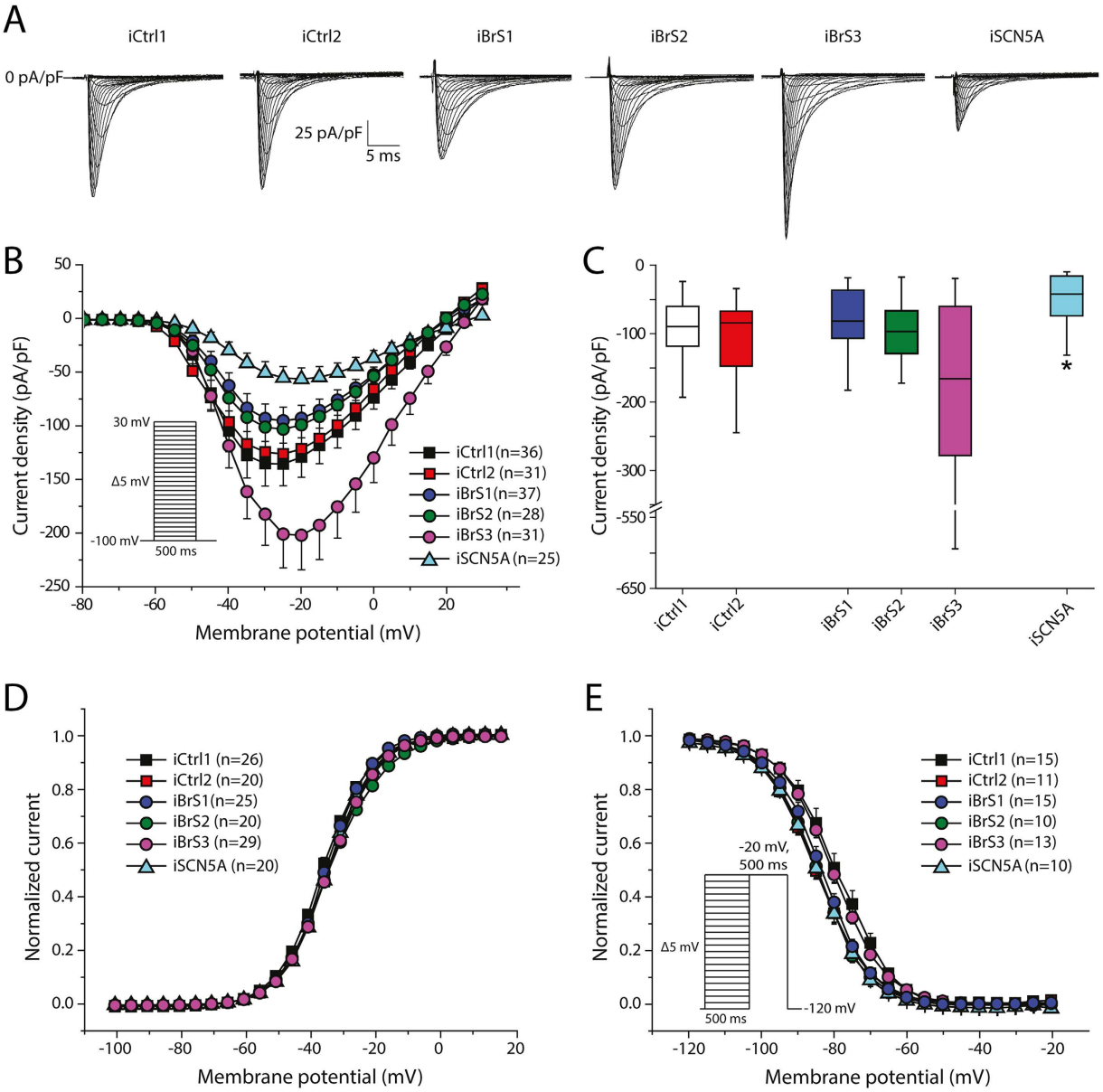

Figure 2. Sodium current (I_{Na}) characterization in hiPSC-CMs from iCtrl1, iCtrl2, the three BrS patients iBrS1 to iBrS3 and iSCN5A. (**A**) Representative traces of I_{Na} as determined by the voltage clamp protocol shown in the inset of (**B**). (**B**) Current-voltage (I-V) relationships of peak I_{Na} (mean ± SEM). (**C**) Boxplots depicting I_{Na} densities (median, boxes represent interquartile range, whiskers 95% interval), determined at −20 mV. *indicates significance compared to iCtrl1 and iCtrl2 ($p < 0.05$; Kruskal-Wallis test, followed by pairwise comparisons). (**D**) Voltage dependence of activation. (**E**) Voltage dependence of inactivation. The inset represents the voltage clamp protocol that was applied.

if a genetic component is operative, it is likely to involve three possibilities. It may entail (1) a non-coding genetic variant that alters the expression of the known BrS associated genes (and thereby acts through effects on the above-mentioned ionic currents), (2) mutations in genes encoding other proteins that affect the above-mentioned or other ionic currents, or alternatively, (3) mutations in genes that act through mechanisms that do not affect cardiomyocyte-intrinsic ion channel dysfunction.

Our electrophysiological studies in hiPSC-CMs from the three mutation-negative BrS patients did not uncover clear cellular electrophysiological differences compared to controls. As loss-of-function of I_{Na} is the most established underlying disease mechanism, we studied this current both directly by means of voltage clamp experiments, and indirectly, by assessment of the upstroke velocity of action potentials. Both methods did not reveal any abnormalities herein. In contrast, in the same experimental system we were able to detect loss of sodium channel function due to the *SCN5A*-1795insD mutation, a genetic defect that gives rise to an overlap phenotype of cardiac sodium channelopathy, encompassing BrS and cardiac conduction disease[19]. hiPSC-CMs

Group	Peak current density (pA/pF) (median ± IQR)	Voltage dependence of activation		Voltage dependence of inactivation		Time dependence of inactivation	
		$V_{1/2}$ (mV)	κ (mV)	$V_{1/2}$ (mV)	κ (mV)	τ_{slow} (ms)	τ_{fast} (ms)
iCtrl1	−93.6 ± 84.9 (n = 36)	−34.6 ± 0.5 (n = 26)	6.9 ± 0.1	−78.9 ± 1.4 (n = 15)*	−6.48 ± 0.2	5.2 ± 0.5 (n = 36)	1.50 ± 0.1
iCtrl2	−83.0 ± 83.3 (n = 31)	−33.0 ± 0.9 (n = 20)	7.0 ± 0.2	−85.0 ± 1.0 (n = 11)	−7.05 ± 0.3	5.9 ± 0.7 (n = 33)	1.50 ± 0.1
iBrS1	−81.7 ± 73.25 (n = 37)	−33.5 ± 0.5 (n = 25)	6.6 ± 0.1	−83.6 ± 0.9 (n = 15)	−6.6 ± 0.2	6.4 ± 0.7 (n = 37)	1.52 ± 0.1
iBrS2	−96.8 ± 70.5 (n = 28)	−34.7 ± 0.7 (n = 20)	7.0 ± 0.2	−84.5 ± 1.0 (n = 10)	−6.6 ± 0.2	7.2 ± 1.0 (n = 31)	1.55 ± 0.1
iBrS3	−151.7 ± 208.5 (n = 31)	−32.1 ± 0.6 (n = 29)	7.2 ± 0.2	−80.0 ± 0.9 (n = 13)†	−6.83 ± 0.2	7.3 ± 0.8 (n = 32)	1.68 ± 0.2
iSCN5A	−38.7 ± 55.03‡ (n = 25)	−31.8 ± 0.9 (n = 20)	6.7 ± 0.2	−83.7 ± 0.8 (n = 10)	−6.9 ± 0.2	16.5 ± 2.0 (n = 25)‡	2.55 ± 0.2‡

Table 1. Sodium current (I_{Na}) density, voltage dependence of (in)activation and time dependence of inactivation from hiPSC-CMs from the two controls (iCtrl1 and iCtrl2), the three BrS patients (iBrS1, iBrS2, iBrS3) and from hiPSC-CMS carrying the mutation 1795insD in *SCN5A* (iSCN5A1795insD). Data is presented as mean ± SEM, unless stated otherwise. $V_{1/2}$, voltage of halfmaximum (in)activation; κ; slope factor of (in)activation; τ_{fast}, fast time constant of inactivation; τ_{slow}, slow time constant of inactivation. *$p < 0.05$ vs. iCtrl2, iBrS1 and iBrS2 (One-way ANOVA, posthoc Bonferroni test). †$p < 0.05$ vs. iCtrl2 (One-way ANOVA, posthoc Bonferroni test). ‡$p < 0.01$ vs. all groups (Kruskal-Wallis test, followed by pairwise comparisons).

carrying this variant (iSCN5A) displayed a clear reduction in I_{Na} density and a decreased AP upstroke velocity as reported previously[17].

Apart from loss-of-function in I_{Na}, loss- and gain-of-function in I_{to} and $I_{Ca,L}$, respectively, have been proposed to contribute to BrS by loss of the AP dome epicardially[20] or by affecting conduction[21]. One out of the three studied BrS cell lines (iBrS2) exhibited a slight reduction in APD, therefore we also studied I_{to} and $I_{Ca,L}$ in this cell line. However, I_{to} and $I_{Ca,L}$ in hiPSC-CMs from iBrS2 demonstrated similar densities and (in)activation properties as compared to the controls. Since we did not assess I_{to} and $I_{Ca,L}$ in hiPSC-CMs from iBrS1 and iBrS3, we cannot completely rule out the possibility that these ion currents are affected in these groups. However, no differences in AP characteristics were observed, suggesting that no marked abnormalities in I_{to} and $I_{Ca,L}$ are present that would contribute to the disease. It can be argued that contribution of I_{to} might be small in APs of hiPSC-CMs[22]; however, due to the *in silico* addition of I_{K1} the MDP in our measurements was negative to −80 mV, a potential were I_{to} is fully available (Fig. 5C). Our observations thus indicate cellular electrophysiological characteristics that do not differ from those of controls, thus supporting the hypothesis that the mechanism(s) underlying the phenotype in these patients may not involve cellular electrophysiological changes and is possibly not caused by mutations in ion channel genes or their modulatory subunits.

In the absence of distinct cellular electrophysiological changes, a number of processes may be hypothesized to contribute, solely or in aggregate, to BrS in these patients. A hypothesis that has increasingly gathered support concerns the role of fibrosis in the right ventricular myocardium[9,10,23,24]. This hypothesis is supported by the fact that BrS typically manifests in the fourth decade of life, which may represent an age at which the development of fibrosis becomes pathogenic. Another mechanism could entail decreased cardiomyocyte coupling through gap junctions[23]. Alternatively, non-genetic/environmental factors might play a more prominent role in these patients. Established modulators in this regard include drugs[25], fever[26] and vagal tone[27]. However, given the high prevalence of positive sodium channel blocker provocation tests in the relatives of the patients we studied (40–50% compared to 4.5% in the general population)[28], a role for genetic factors seems likely. Lastly, BrS may be a multifactorial disorder, wherein multiple genetic and environmental factors each contribute to varying extent[29]. In such a scenario, small-effect defects in the ionic currents that shape the action potential might have been missed in the hiPSC-CM system we used.

Although our results indicate a lack of ion channel dysfunction in the three BrS patients, some considerations should be taken into account. It is well established that hiPSC-CMs exhibit electrophysiological characteristics that are comparable to fetal cardiomyocytes[30]. In our study, we partly corrected the electrophysiological immaturity by the *in silico* injection of I_{K1}[31], which consistently results in action potentials with a physiological resting membrane potential, thereby attaining physiological availability of I_{Na} and I_{to}. However, important factors that modulate ion channel expression and function, such as beta subunits, transcription factors, microRNAs and epigenetic profile, may differ from mature cardiomyocytes[30]. Another feature of hiPSC-CMs is the lack of a defined intercalated disc, which in adult cardiomyocytes contains a distinct pool of sodium channels that have macromolecular interactions that differ compared to those at the lateral membrane[32]. Abnormalities in any of the proteins that are involved in the formation and maintenance of these distinct pools of sodium channels could be masked in hiPSC-CMs. In BrS, electrophysiological abnormalities including arrhythmia originate from the right ventricular outflow tract[8,33]. The transcriptome of cardiomyocytes from this region differs from that of other regions of the heart[34] and this may confer different functional characteristics. The fate heterogeneity in cardiomyocyte populations derived by differentiation from hiPSC necessitates the use of specific culture protocols to enrich for specific cardiomyocyte subtypes. While differentiation protocols enriching for atrial-like cardiomyocytes[35] and cardiomyocytes with properties of sinoatrial node cells[36] have been developed, these are as yet not available for the right ventricular outflow tract. Notwithstanding, in our system we could recapitulate the effects of a BrS-causing *SCN5A* mutation.

In line with the cellular heterogeneity, we observed a high degree of variability in I_{Na}, which could mask subtle differences in this current. However, one should note that AP upstroke velocities, reflecting sodium channel functionality, displayed less variation, possibly due to the selection of viable, regularly beating cells. The fact that

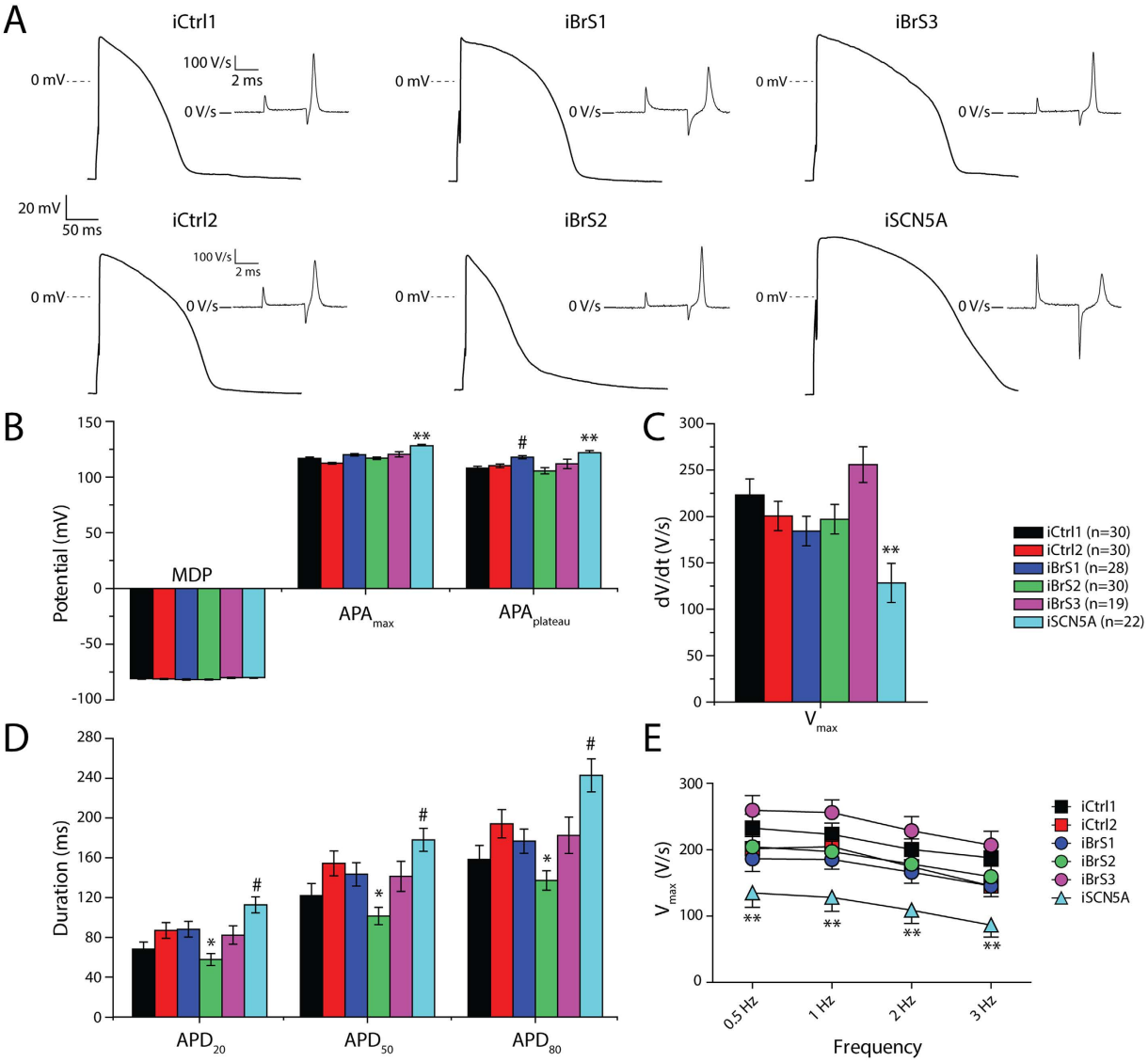

Figure 3. AP characteristics as measured after addition of *in silico* I_{K1} in hiPSC-CMs from iCtrl1, iCtrl2, the three BrS patients iBrS1 to iBrS3 and iSCN5A. (**A**) Typical examples of APs measured at 1 Hz. Inset show the first derivatives displaying AP upstroke velocity. (**B**) Averages of maximum diastolic potential (MDP), maximum AP amplitude (APA_{max}) and amplitude of the plateau ($APA_{plateau}$), measured after 10 ms from the onset of the upstroke. (**C**) Maximal upstroke velocity (V_{max}) at 1 Hz. V_{max} in hiPSC-CMs from iBrS1, iBrS2 and iBrS3 is not significantly different from iCtrl1 and iCtrl2, in contrast to iSCN5A, which shows a marked reduction ($p < 0.05$; ANOVA, followed by Bonferroni posthoc tests). (**D**) Action potential duration (APD) at 20, 50 and 80% of repolarization (APD_{20}, APD_{50} and APD_{80}, respectively). APD is reduced in iBrS2 compared to iCtrl2 ($p < 0.05$), while iSCN5A exhibits an increase in APD compared to iCtrl1 ($p < 0.05$; ANOVA, followed by Bonferroni posthoc tests). (**E**) Rate dependency of V_{max} at frequencies of 0.5 to 3 Hz. No additional differences are exposed at higher or lower frequencies. **$p < 0.05$ vs iCtrl1 and iCtrl2. $^{\#}p < 0.05$ vs iCtrl1 *$p < 0.05$ vs iCtrl2.

no differences were observed in the latter parameter, which is more sensitive for the detection of small effects, supports our notion that I_{Na} is not affected in hiPSC-CMs from the selected BrS patients.

So far, electrophysiological studies in hiPSC-CMs have been mainly conducted in hiPSC-CMs derived from patients with known genetic defects and have mainly focused on the recapitulation of electrophysiological defects that had been previously described in other model systems such as heterologous expression systems or mouse models[17,37,38]. Our study for the first time attempts to glean insight into the mechanism of a cardiac disease in patients in which the underlying genetic defect is not known.

In conclusion, our study of hiPSC-CMs from three unrelated BrS patients without *SCN5A* mutations does not point towards an ion channel defect as a mechanism that contributes to the disease. This suggests that other pathophysiological mechanisms could be operative in these patients.

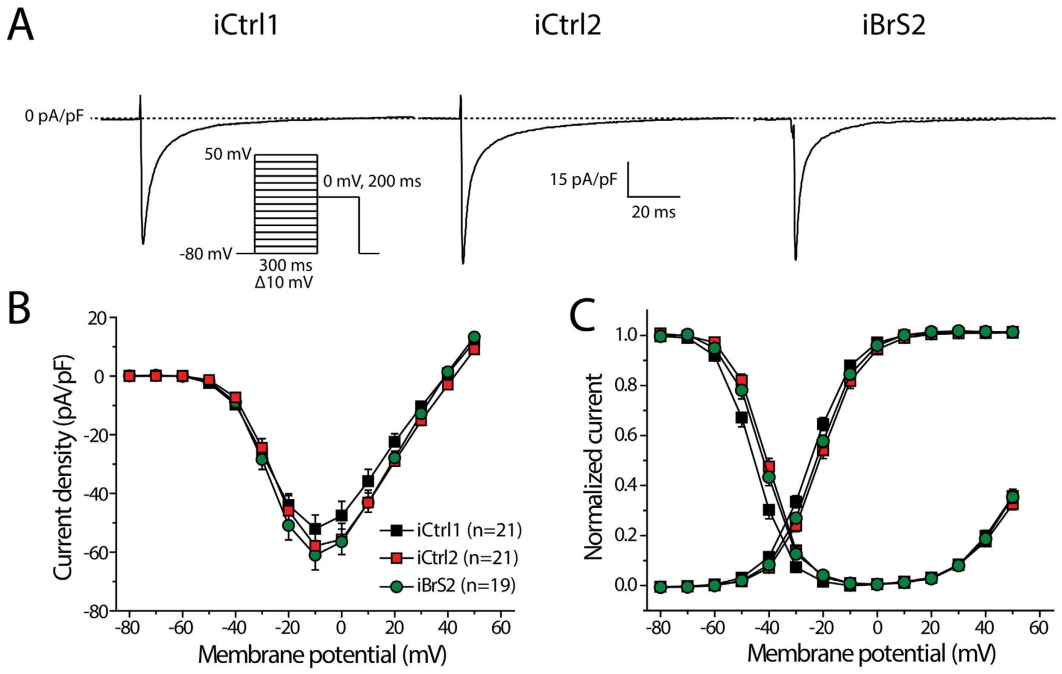

Figure 4. L-type calcium current ($I_{Ca,L}$) in hiPSC-CMs from iCtrl1, iCtrl2 and iBrS2. (**A**) Typical traces of $I_{Ca,L}$ measured at a test potential of 0 mV. Inset shows the used voltage clamp protocol. (**B**) I-V relationships of $I_{Ca,L}$. (**C**) Voltage dependence of activation and inactivation.

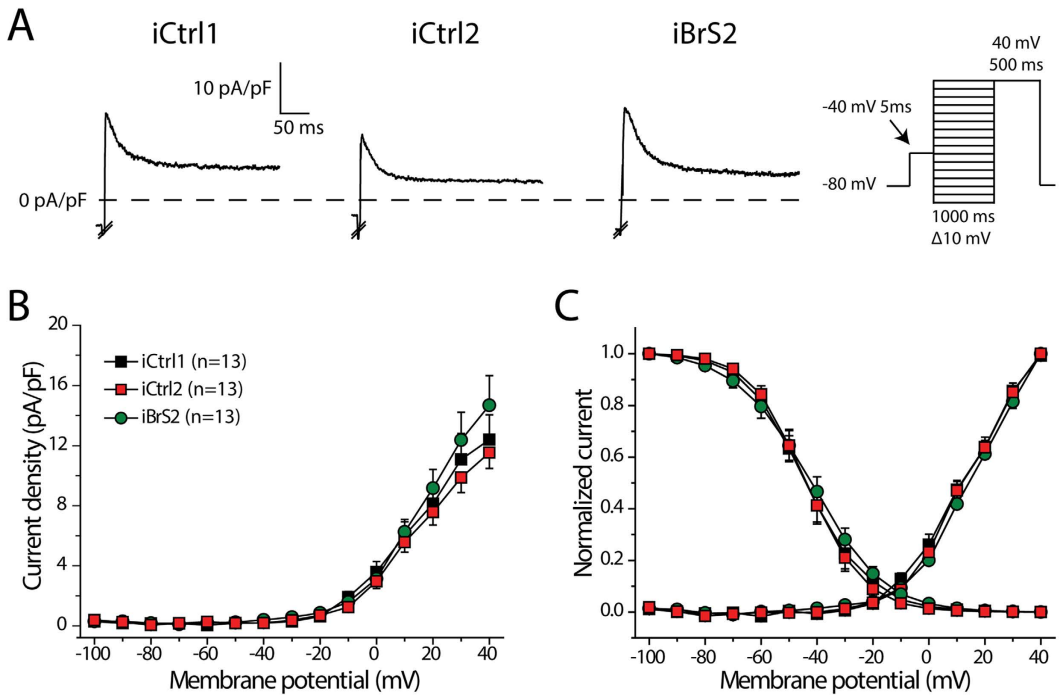

Figure 5. Transient outward potassium current (I_{to}) in hiPSC-CMs from iCtrl1, iCtrl2 and iBrS2. (**A**) Representative trances of I_{to} elicited at a test potential of +40 mV. Inset shows the voltage clamp protocol, in which a prepulse of 5 ms to −40 is applied to activate and inactivate I_{Na}. Please note that I_{Na} was cut-off in the depicted examples. (**B**) I-V relationships of I_{to}. No statistical differences are present (One-Way Anova, $p > 0.05$) (**C**) Voltage dependence of activation and inactivation.

Methods

Genetic screening. The coding regions and splice sites of genes previously associated with BrS were screened for novel and rare variants in the 3 BrS patients by a next-generation sequencing (NGS) approach we used

previously[39]. These genes were *SCN5A, SCN1B*, *SCN2B*, *SCN3B, SCN10A, CACNA1C*, *CACNB2*, *CACNA2D1, KCNH2*, *KCNE3*, *KCNE1L*, *KCND3*, *KCNJ8, ABCC9, TRPM4*, *HCN4, GPD1L*, *RANGRF*, *PKP2* and *FGF12*. The coding exons and flanking splice sites were captured from 200 ng of genomic DNA using the Agilent HaloPlex Target Enrichment system (Agilent Technologies) following the manufacturer's protocol. 100-bp paired end read sequencing was conducted on a HiSeq sequencer (Illumina). Sequence reads were aligned to the human reference genome (standard 1000Genomes fasta GRCh37 alignment file) using BWA (version 0.6.2)[40] and called using GATK (version 2.6)[41] and SAMtools (version 0.1.19)[42]. On average, the mean depth was 503, and 96.4% of the targeted regions were covered at least 10 times. The Knime4Bio tool was used to manage and filter variants[43]. Synonymous variations that were not located at splice sites were excluded from further analysis. Heterozygous and homozygous coding and splice site variants with a minor allele frequency (MAF) below 1% in public databases (Exome Aggregation Consortium (ExAC), Cambridge, MA (URL: http://exac.broadinstitute.org), GoNL[44] and the 69 genomes from Complete Genomics) were retained and validated by Sanger sequencing.

Generation and characterization of hiPSC. The study was approved by the ethics committee of the Academic Medical Center of the University of Amsterdam (Netherlands) and conducted according to the approved guidelines. Informed consent was obtained from all study objects. The two control hiPSC lines (iCTRL1 and 2) and the hiPSC line carrying the *SCN5A*-1795insD mutation (i*SCN5A*) were generated and characterized previously[17,45,46]. Patient hiPSC lines (iBrS1-3) were generated from fibroblasts derived from skin punch biopsies. Dermal fibroblasts from the three patients were reprogrammed using the lentiviral STEMCCA system carrying the OCT4, KLF4, SOX2 and cMYC factors as previously described[45]. Pluripotency of the generated lines was confirmed by alkaline phosphatase staining, and by immunocytochemistry and RT-PCR for the detection of expression of the pluripotency markers OCT4, SOX2, NANOG, LIN28, SSEA-4, and TRA-1-60. The related primers, antibodies and applied protocols are described previously[45]. For each line, the potential to generate cell types derived from the three germ layers was tested by immunocytochemistry for the markers β-III-Tubulin, α-SMA and AFP after spontaneous differentiation of the hiPSC. Karyotype analysis was performed by the COBRA-FISH technique[47].

Differentiation of hiPSCs into cardiomyocytes and dissociation in single cells. All hiPSC lines were expanded as adherent cultures in feeder-free conditions on Matrigel-coated dishes in the presence of chemically defined medium (E8 Essential Medium, Life Technologies). Differentiation of hiPSC to cardiomyocytes (CMs) was performed over a period of 30 days following a previously reported protocol[48] based on small molecules-mediated canonical Wnt pathway modulation (see Supplementary methods for more detail). Subsequently we enriched for CMs by switching the culture medium to DMEM supplemented with lactic acid (4 mmol/L) in substitution of glucose for 6 days as previously reported[49]. Cultures of hiPSC-CMs were then enzymatically dissociated into single cells using Elastase (Serva) and Liberase (Roche Chemicals) as described previously[31]. CMs were stained with anti-NKX-2.5 and cardiac TroponinT antibodies as described in the Supplementary methods. To allow for single-cell electrophysiological measurements, dissociated cells were plated at a low density on Matrigel-coated coverslips. Electrophysiological measurements were performed 9–14 days after dissociation.

Electrophysiology. *Data acquisition and analysis.* Action potentials (APs) and I_{Na} were recorded using an Axopatch 200 B amplifier (Molecular Devices, Sunnyvale, CA, USA). Voltage control, data acquisition, and analysis were realized with custom software. Potentials were corrected for the calculated liquid junction potentials. Cell membrane capacitance (C_m) was calculated by dividing the time constant of the decay of the capacitive transient after a −5 mV voltage step from −50 mV by the series resistance. Signals were low-pass-filtered with a cutoff of 5 kHz and digitized at 40 kHz for APs, 20 kHz for I_{Na}, 10 kHz for $I_{Ca,L}$ and 4 kHz for I_{to}. For all lines and experiments, data was collected from at least 3 independent differentiations.

Action potentials. AP measurements were acquired at 36 ± 0.2 °C from single hiPSC-CMs using the amphotericin-B-perforated patch-clamp technique. Spontaneously beating hiPSC-CMS showing regular, synchronous contractions were selected. Pipettes (borosylicate glass) were filled with solution containing (in mmol/L): 125 K-gluconate, 20 KCl, 10 NaCl, 0.44 amphotericin-B, 10 HEPES; pH 7.2 (KOH). Bath solution contained (in mM): 140 NaCl, 5.4 KCl, 1.8 $CaCl_2$, 1.0 $MgCl_2$, 5.5 glucose, 5.0 HEPES; pH 7.4 (NaOH). Typically, hiPSC-CMs have a small or even complete lack of the inward rectifying potassium current (I_{K1})[31]. Consequently, hiPSC-CMs have a depolarized maximal diastolic potential (MDP) and are frequently spontaneously active[30]. To overcome these conditions, which limit the functional availability of I_{Na} and I_{to}, we injected an *in silico* I_{K1} with kinetics of $Kir_{2.1}$ channels through dynamic clamp, as previously described in detail[31]. In the present study, we consistently used an amount of 2 pA/pF peak outward current which resulted in quiescent hiPSC-CMs with a RMP of −80 mV or more negative that displayed ventricular-like APs in >90% of the cells (based on the proportion of cells with a plateau amplitude of >85 mV, measured 20 ms after the initiation of the AP upstroke; see Supplementary Fig. 7). The proportion of hiPSC-CMs displaying ventricular-like AP was not different between the groups. Because the vast majority of cells exhibited ventricular-like APs and a selection of hiPSC-CMs subtypes cannot be achieved during ion current measurements, we refrained from performing a selection based on action potential morphology. Action potentials were elicited at 0.5 to 3 Hz by 3-ms, ~1.2x threshold current pulses through the patch pipette. APs were characterized by MDP, maximum AP amplitude (APA_{max}), AP duration at 20, 50 and 80% of repolarization (APD_{20}, APD_{50}, APD_{80} respectively), maximal upstroke velocity (V_{max}) and plateau amplitude ($APA_{plateau}$, measured 20 ms after the AP upstroke). Averages were taken from 10 consecutive APs and cells with an access resistance of >50 MΩ were excluded from analysis.

Membrane currents. I_{Na}, $I_{Ca,L}$ and I_{to} were measured using the ruptured patch-clamp technique with conventional voltage clamp protocols as depicted in the accompanying figures. I_{Na} was measured at room temperature, $I_{Ca,L}$ and I_{to} were measured at 36 ± 0.2 °C. Cycle lengths were 5, 2 and 10 seconds for I_{Na}, $I_{Ca,L}$ and I_{to}, respectively. I_{Na}, $I_{Ca,L}$ and I_{to} were defined as the difference between peak current and steady-state current. Current densities were calculated by dividing currents by C_M. Steady-state activation and inactivation curves were fitted by using a Boltzmann equation: $I/I_{max} = A/\{1.0 + \exp[(V_{1/2} - V)/k]\}$. In which $V_{1/2}$ is half-maximum (in)activation potential and k is the slope factor. For voltage dependence of (in)activation of I_{Na}, only cells with adequate voltage control were included, as ascertained by a slope factor >6 for both activation and inactivation. Time constants of inactivation of I_{Na} and $I_{Ca,L}$ were determined by fitting a biexponential curve through the decay phase of the current using the equation: $I/I_{max} = A_f \times \exp(-t/\tau_f) + A_s \times \exp(-t/\tau_s)$, in which A_f and A_s are the fractions of the fast and slow inactivation components, and τ_f and τ_s are the time constants of the fast and slow inactivating components, respectively. Time constants of inactivation of I_{to} was fitted with a mono-exponential equation. For I_{Na}, pipette solutions contained (in mmol/L): 3.0 NaCl, 133 CsCl, 2.0 $MgCl_2$, 2.0 Na_2ATP, 2.0 TEACl, 10 EGTA, 5.0 HEPES; pH 7.2 (CsOH). Bath solution for I_{Na} contained (in mmol/L)): 20 NaCl, 120 CsCl, 1.8 $CaCl_2$, 1.2 $MgCl_2$, 11.0 glucose, 5.0 HEPES; nifedipine 0.01; pH 7.4 (CsOH). For $I_{Ca,L}$ and I_{to}, spontaneously beating cells were selected in the same bath solution as used for APs after which the solutions were switched to specific extracellular solutions. $I_{Ca,L}$ was measured in a bath solution containing (in mmol/L): 145 TEA-Cl, 5.4 CsCl, 1.8 $CaCl_2$, 1.0 $MgCl_2$, 5.0 HEPES, pH 7.4 (NMDG-OH). For I_{to} measurements, bath solution, was the same as for APs, except that 0.5 mM $CdCl_2$ was added to block $I_{Ca,L}$ and reduce I_{Na}. For $I_{Ca,L}$ measurements, pipettes were filled with solutions containing (in mmol/L): 145 CsCl, 10 HEPES, 10 EGTA, 5 K_2ATP, pH 7.2 (NMDG-OH). Pipette solution for I_{to} measurements contained (in mmol/L): 105 K-gluconate, 20 KCl, 5 NaCl, 1 $MgCl_2$, 10 BAPTA (pre-dissolved in KOH), 5 MgATP, 10 HEPES, pH 7.2 (NMDG-OH).

Statistics. Statistical analysis was performed with SPSS Statistics 22. Normality and equality of variance were tested by Shapiro-Wilk and Levene median test, respectively. For parameters with a normal distribution, One-Way ANOVA followed by Bonferroni *post hoc* tests were performed. In case of non-normally distributed parameters, Kruskal-Wallis tests followed by pairwise comparisons with Bonferroni error corrections were applied. In all tests, comparisons were done between the test group (i.e. iBrS1, iBrS2, iBrS3 or iSCN5A) and the two controls (i.e. iCtrl1 and iCtrl2). For frequency dependence among groups, Two-Way repeated measures ANOVA was used. Data are presented as mean ± SEM, unless stated otherwise. $P < 0.05$ defines statistical significance.

References

1. Brugada, P. & Brugada, J. Right bundle branch block, persistent ST segment elevation and sudden cardiac death: a distinct clinical and electrocardiographic syndrome. A multicenter report. *J Am Coll Cardiol* **20,** 1391–1396 (1992).
2. Mizusawa, Y. & Wilde, A. A. Brugada syndrome. *Circ Arrhythm Electrophysiol* **5,** 606–616 (2012).
3. Crotti, L. *et al.* Spectrum and prevalence of mutations involving BrS1- through BrS12-susceptibility genes in a cohort of unrelated patients referred for Brugada syndrome genetic testing: implications for genetic testing. *J Am Coll Cardiol* **60,** 1410–1418 (2012).
4. Le Scouarnec, S. *et al.* Testing the burden of rare variation in arrhythmia-susceptibility genes provides new insights into molecular diagnosis for Brugada syndrome. *Hum Mol Genet* **24,** 2757–2763 (2015).
5. Gellens, M. E. *et al.* Primary structure and functional expression of the human cardiac tetrodotoxin-insensitive voltage-dependent sodium channel. *Proc. Natl. Acad. Sci. USA* **89,** 554–558 (1992).
6. Hoogendijk, M. G. *et al.* The Brugada ECG pattern: a marker of channelopathy, structural heart disease, or neither? Toward a unifying mechanism of the Brugada syndrome. *Circ Arrhythm Electrophysiol* **3,** 283–290 (2010).
7. Koopmann, T. T. *et al.* Exclusion of multiple candidate genes and large genomic rearrangements in SCN5A in a Dutch Brugada syndrome cohort. *Heart Rhythm* **4,** 752–755 (2007).
8. Nademanee, K. *et al.* Prevention of ventricular fibrillation episodes in Brugada syndrome by catheter ablation over the anterior right ventricular outflow tract epicardium. *Circulation* **123,** 1270–1279 (2011).
9. Catalano, O. *et al.* Magnetic resonance investigations in Brugada syndrome reveal unexpectedly high rate of structural abnormalities. *Eur Heart J* **30,** 2241–2248 (2009).
10. Coronel, R. *et al.* Right ventricular fibrosis and conduction delay in a patient with clinical signs of Brugada syndrome: a combined electrophysiological, genetic, histopathologic, and computational study. *Circulation* **112,** 2769–2777 (2005).
11. Hoekstra, M., Mummery, C. L., Wilde, A. A., Bezzina, C. R. & Verkerk, A. O. Induced pluripotent stem cell derived cardiomyocytes as models for cardiac arrhythmias. *Front Physiol* **3,** 346 (2012).
12. Antzelevitch, C. *et al.* Brugada syndrome: report of the second consensus conference: endorsed by the Heart Rhythm Society and the European Heart Rhythm Association. *Circulation* **111,** 659–670 (2005).
13. Postema, P. G. & Wilde, A. A. The measurement of the QT interval. *Curr Cardiol Rev* **10,** 287–294 (2014).
14. Desmet, F. O. *et al.* Human Splicing Finder: an online bioinformatics tool to predict splicing signals. *Nucleic Acids Res* **37,** e67 (2009).
15. Wang, M. & Marin, A. Characterization and prediction of alternative splice sites. *Gene* **366,** 219–227 (2006).
16. Reese, M. G., Eeckman, F. H., Kulp, D. & Haussler, D. Improved splice site detection in Genie. *J Comput Biol* **4,** 311–323 (1997).
17. Davis, R. P. *et al.* Cardiomyocytes derived from pluripotent stem cells recapitulate electrophysiological characteristics of an overlap syndrome of cardiac sodium channel disease. *Circulation* **125,** 3079–3091 (2012).
18. Berecki, G., Wilders, R., de Jonge, B., van Ginneken, A. C. & Verkerk, A. O. Re-evaluation of the action potential upstroke velocity as a measure of the Na+ current in cardiac myocytes at physiological conditions. *PLoS One* **5,** e15772 (2010).
19. Bezzina, C. *et al.* A single Na(+) channel mutation causing both long-QT and Brugada syndromes. *Circ Res* **85,** 1206–1213 (1999).
20. Antzelevitch, C. Cellular basis and mechanism underlying normal and abnormal myocardial repolarization and arrhythmogenesis. *Ann Med* **36** Suppl 1, 5–14 (2004).
21. Huelsing, D. J., Spitzer, K. W., Cordeiro, J. M. & Pollard, A. E. Conduction between isolated rabbit Purkinje and ventricular myocytes coupled by a variable resistance. *Am J Physiol* **274,** H1163–1173 (1998).
22. Cordeiro, J. M. *et al.* Identification and characterization of a transient outward K+ current in human induced pluripotent stem cell-derived cardiomyocytes. *J Mol Cell Cardiol* **60,** 36–46 (2013).
23. Nademanee, K. *et al.* Fibrosis, Connexin-43, and Conduction Abnormalities in the Brugada Syndrome. *J Am Coll Cardiol* **66,** 1976–1986 (2015).
24. Hoogendijk, M. G. *et al.* Mechanism of right precordial ST-segment elevation in structural heart disease: excitation failure by current-to-load mismatch. *Heart Rhythm* **7,** 238–248 (2010).

25. Postema, P. G. *et al.* Drugs and Brugada syndrome patients: review of the literature, recommendations, and an up-to-date website (www.brugadadrugs.org). *Heart Rhythm* **6,** 1335–1341 (2009).
26. Amin, A. S., Meregalli, P. G., Bardai, A., Wilde, A. A. & Tan, H. L. Fever increases the risk for cardiac arrest in the Brugada syndrome. *Ann Intern Med* **149,** 216–218 (2008).
27. Matsuo, K. *et al.* The circadian pattern of the development of ventricular fibrillation in patients with Brugada syndrome. *Eur Heart J* **20,** 465–470 (1999).
28. Hasdemir, C. *et al.* High prevalence of concealed Brugada syndrome in patients with atrioventricular nodal reentrant tachycardia. *Heart Rhythm* **12,** 1584–1594 (2015).
29. Bezzina, C. R. *et al.* Common variants at SCN5A-SCN10A and HEY2 are associated with Brugada syndrome, a rare disease with high risk of sudden cardiac death. *Nat Genet* **45,** 1044–1049 (2013).
30. Veerman, C. C. *et al.* Immaturity of human stem-cell-derived cardiomyocytes in culture: fatal flaw or soluble problem? *Stem Cells Dev* **24,** 1035–1052 (2015).
31. Meijer van Putten, R. M. *et al.* Ion channelopathies in human induced pluripotent stem cell derived cardiomyocytes: a dynamic clamp study with virtual IK1. *Front Physiol* **6,** 7 (2015).
32. Petitprez, S. *et al.* SAP97 and dystrophin macromolecular complexes determine two pools of cardiac sodium channels Nav1.5 in cardiomyocytes. *Circ Res* **108,** 294–304 (2011).
33. Zhang, J. *et al.* Cardiac electrophysiological substrate underlying the ECG phenotype and electrogram abnormalities in Brugada syndrome patients. *Circulation* **131,** 1950–1959 (2015).
34. Boukens, B. J., Christoffels, V. M., Coronel, R. & Moorman, A. F. Developmental basis for electrophysiological heterogeneity in the ventricular and outflow tract myocardium as a substrate for life-threatening ventricular arrhythmias. *Circ Res* **104,** 19–31 (2009).
35. Devalla, H. D. *et al.* Atrial-like cardiomyocytes from human pluripotent stem cells are a robust preclinical model for assessing atrial-selective pharmacology. *EMBO Mol Med* **7,** 394–410 (2015).
36. Birket, M. J. *et al.* Expansion and patterning of cardiovascular progenitors derived from human pluripotent stem cells. *Nat Biotechnol* **33,** 970–979 (2015).
37. Moretti, A. *et al.* Patient-specific induced pluripotent stem-cell models for long-QT syndrome. *N Engl J Med* **363,** 1397–1409 (2010).
38. Zhang, M. *et al.* Recessive cardiac phenotypes in induced pluripotent stem cell models of Jervell and Lange-Nielsen syndrome: disease mechanisms and pharmacological rescue. *Proc Natl Acad Sci USA* **111,** E5383–5392 (2014).
39. Marsman, R. F. *et al.* A mutation in CALM1 encoding calmodulin in familial idiopathic ventricular fibrillation in childhood and adolescence. *J Am Coll Cardiol* **63,** 259–266 (2014).
40. Li, H. & Durbin, R. Fast and accurate short read alignment with Burrows-Wheeler transform. *Bioinformatics* **25,** 1754–1760 (2009).
41. McKenna, A. *et al.* The Genome Analysis Toolkit: a MapReduce framework for analyzing next-generation DNA sequencing data. *Genome Res* **20,** 1297–1303 (2010).
42. Li, H. *et al.* The Sequence Alignment/Map format and SAMtools. *Bioinformatics* **25,** 2078–2079 (2009).
43. Lindenbaum, P., Le Scouarnec, S., Portero, V. & Redon, R. Knime4Bio: a set of custom nodes for the interpretation of next-generation sequencing data with KNIME. *Bioinformatics* 27, 3200–3201 (2011).
44. Boomsma, D. I. *et al.* The Genome of the Netherlands: design, and project goals. *Eur J Hum Genet* **22,** 221–227 (2014).
45. Streckfuss-Bomeke, K. *et al.* Comparative study of human-induced pluripotent stem cells derived from bone marrow cells, hair keratinocytes, and skin fibroblasts. *Eur Heart J* **34,** 2618–2629 (2013).
46. Dudek, J. *et al.* Cardiolipin deficiency affects respiratory chain function and organization in an induced pluripotent stem cell model of Barth syndrome. *Stem Cell Res* **11,** 806–819 (2013).
47. Szuhai, K. & Tanke, H. J. COBRA: combined binary ratio labeling of nucleic-acid probes for multi-color fluorescence *in situ* hybridization karyotyping. *Nat Protoc* **1,** 264–275 (2006).
48. Lian, X. *et al.* Directed cardiomyocyte differentiation from human pluripotent stem cells by modulating Wnt/beta-catenin signaling under fully defined conditions. *Nat Protoc* **8,** 162–175 (2013).
49. Tohyama, S. *et al.* Distinct metabolic flow enables large-scale purification of mouse and human pluripotent stem cell-derived cardiomyocytes. *Cell Stem Cell* **12,** 127–137 (2013).

Acknowledgements

We thank Dr. Richard Redon, Dr. Pierre Lindenbaum and Dr. Stephanie Bonnaud (Genomics Core Facility, University of Nantes) for the Haloplex targeted capture and NGS in the Brugada Syndrome patients. We thank Prof. Christine Mummery and Dr. Christian Freund (Dept. of Anatomy & Embryology, Leiden University Medical Center) for the generation of the iSCN5A hiPSC line. This work was funded by the Rembrandt Institute for Cardiovascular Sciences, the CardioVascular Onderzoek Nederland and Netherlands Heart Foundation project PREDICT, and a Netherlands Organization for Scientific Research (NWO) VICI grant (016.150.610) to C.R. Bezzina.

Author Contributions

C.C.V., I.M., A.O.V. and C.R.B. conceived and designed the experiments. C.C.V., I.M., A.O.V. and M.S. conducted the experiments. Data were analyzed by C.C.V., J.B, A.O.V., K.G. and H.L.T. provided reagents/materials/ analysis tools. C.C.V., A.O.V., A.A.M.W. and C.R.B. wrote the manuscript. All authors reviewed and contributed to the final version of the manuscript.

Additional Information

Supplementary information accompanies this paper at http://www.nature.com/srep

Competing financial interests: The authors declare no competing financial interests.

How to cite this article: Veerman, C. C. *et al.* hiPSC-derived cardiomyocytes from Brugada Syndrome patients without identified mutations do not exhibit clear cellular electrophysiological abnormalities. *Sci. Rep.* **6**, 30967; doi: 10.1038/srep30967 (2016).